Mechanosensor Piezo1-mediated smooth muscular cell pyroptosis contributes to vascular calcification

JUN TAO[1,2*], DAITING YOU[1*], ZEJIANG FENG[1], HUANGJING LI[1], YAO ZHANG[2], YUTING CUI[2], KAIYUAN LIN[2], BIN LUO[3], SHENGLI YIN[4] and HONGMEI TAN[1]

[1]Department of Pathophysiology, School of Medicine, Shenzhen Campus of Sun Yat-sen University, Shenzhen, Guangdong 518107, P.R. China; [2]Department of Pathophysiology, Zhongshan School of Medicine, Sun Yat-sen University, Guangzhou, Guangdong 510080, P.R. China; [3]Department of Forensic Medicine, Zhongshan School of Medicine, Sun Yat-sen University, Guangzhou, Guangdong 510080, P.R. China; [4]Department of Cardiac Surgery, Hui Ya Hospital of The First Affiliated Hospital, Sun Yat-sen University, Huizhou, Guangdong 516081, P.R. China

Received March 8, 2025; Accepted July 8, 2025

DOI: 10.3892/ijmm.2025.5637

Abstract. Vascular calcification is a pathological consequence of chronic inflammation and phenotypic switching in smooth muscle cells (SMCs). However, the mechanisms underlying vascular calcification remain unclear. The present study explores the role of the mechanosensor channel, Piezo1, in regulating vascular SMC (VSMC) death and vascular calcification. The findings of the present study demonstrated that Piezo1 expression is upregulated in the atherosclerotic plaques of both mice and patients. *In vitro* experiments revealed that calcifying medium (CM) induced an increase in Piezo1 and runt-related transcription factor 2 (RUNX2) expression, triggered pyroptosis in cultured VSMCs and promoted calcium deposition in arterial rings. These effects were mitigated by a Piezo1 inhibitor and exacerbated by a Piezo1 agonist. Furthermore, gene deletion of NLR family pyrin domain containing 3 (NLRP3), caspase1 or gasdermin D also reduced CM-induced pyroptosis and calcium deposition in VSMCs. Immunoprecipitation assays showed that calcium/calmodulin dependent protein kinase II (CaMKII), a downstream effector of Piezo1, interacted with RUNX2, and CaMKII inhibition attenuated both pyroptosis and calcification in VSMCs exposed to CM. The role of Piezo1 in mediating VSMC pyroptosis and vascular calcification was confirmed in a mouse model, where VSMC-specific deletion of Piezo1 inhibited arterial calcification in chronic kidney disease. In conclusion, Piezo1 is a key regulator of vascular calcification via Ca^{2+}-CaMKII-mediated activation of the NLRP3 inflammasome and subsequent VSMC pyroptosis.

Correspondence to: Professor Hongmei Tan, Department of Pathophysiology, School of Medicine, Shenzhen Campus of Sun Yat-sen University, 66 Gongchang Road, Guangming, Shenzhen, Guangdong 518107, P.R. China
E-mail: tanhm@mail.sysu.edu.cn

Professor Shengli Yin, Department of Cardiac Surgery, Hui Ya Hospital of The First Affiliated Hospital, Sun Yat-sen University, 86 Zhongxing North Road, Daya Bay, Huizhou, Guangdong 516081, P.R. China
E-mail: yshengl03@163.com

*Contributed equally

Key words: arterial calcification, Piezo1, NLR family pyrin domain containing 3, pyroptosis, vascular smooth muscle cells, calcium/calmodulin dependent protein kinase II

Introduction

Arterial calcification is marked by abnormal calcium deposition and increased arterial stiffness, commonly observed in patients with atherosclerosis or chronic kidney disease (CKD); it is strongly linked to oxidative stress, chronic inflammation and abnormal cell death, all of which contribute to heightened cardiovascular risk (1). A key initiating event in vascular calcification is the phenotypic switch of vascular smooth muscle cells (VSMCs) into osteoblast-like cells. This transformation is characterized by the loss of VSMC-specific markers and the acquisition of osteochondrogenic markers such as runt-related transcription factor 2 (RUNX2) and bone morphogenetic protein 2 (BMP2), along with aberrant VSMC death (2). Inflammation acts as both a trigger and consequence of calcification, creating a potentially vicious cycle between inflammatory processes and arterial calcification. Calcium phosphate crystals, which function as danger-associated molecular patterns (DAMPs), activate caspase1 and promote the maturation of interleukin-1β (IL-1β), initiating a pro-inflammatory cascade (3). A study has shown increased IL-1β expression in CKD models with vascular calcification, underscoring the pivotal role of inflammation in this pathology (4). Nonetheless, the extent to which suppressing inflammation in VSMCs might mitigate vascular calcification remains largely unresolved.

Pyroptosis, a form of regulated cell death, was initially identified as pro-inflammatory cell death in *Salmonella*-infected macrophages (5). This form of cell death is driven by inflammatory caspases, primarily caspase1, which activate inflammatory cytokines and induce cell death, largely

mediated by inflammasomes (6). The NLR family pyrin domain containing 3 (NLRP3) inflammasome is composed of NLRP3, caspase1 and apoptosis-associated speck-like protein containing a caspase recruitment domain (ASC). A priming event stimulates the transcription of NLRP3 and precursors of caspase1 (pro-caspase1) and IL-1β (pro-IL-1β) via toll-like receptor (TLR) and nuclear factor κB signaling. The subsequent assembly of NLRP3, ASC and pro-caspase1 leads to the formation of the NLRP3 inflammasome, triggering auto-cleavage of pro-caspase1 and the maturation of pro-IL-1β and pro-IL-18 (7). Simultaneously, caspase1 cleaves gasdermin D (GSDMD), generating an N-terminal GSDMD fragment (GSDMD-NT) that forms pores in the plasma membrane, facilitating pyroptotic cell death (8). Pyroptosis has been implicated in the progression of several diseases, including cardiovascular disease, diabetes and neurological disorders (9). In cardiovascular contexts, NLRP3 inflammasome activation has been shown to regulate VSMC phenotypic switching in conditions such as atherosclerosis and abdominal aortic aneurysms (10,11). However, its specific role in VSMCs during arterial calcification remains unclear.

Piezo1 is a non-selective, mechanically gated cation channel that converts mechanical stimuli into electrochemical signals by facilitating the influx of cations such as calcium, sodium and potassium across various cell types, including endothelial cells, red blood cells and SMCs (12-14). This mechanotransduction is involved in several physiological and pathological processes, such as the development of blood and lymphatic vessels (12,13), the regulation of vascular tone (15,16) and arterial remodeling (15). Additionally, Piezo1-induced Ca^{2+} influx plays a critical role in the functions of macrophages, particularly in inflammatory activation (17). As a key intracellular second messenger, Ca^{2+} is essential for calcium/calmodulin dependent protein kinase II (CaMKII) activation. Upon binding to the regulatory domain of CaMKII, Ca^{2+} triggers autophosphorylation at threonine 286, leading to its sustained activation. CaMKII is widely recognized as a key downstream effector of Piezo1 signaling (18,19). Previous research has shown that Piezo1 contributes to the pathology of aortic aneurysms and that inhibiting Piezo1 reduces atherosclerotic plaque formation in mice (20). However, its involvement in the inflammatory response and pyroptosis during arterial calcification remains unexplored.

The present study aims to determine whether Piezo1 modulates NLRP3 inflammasome-mediated VSMC pyroptosis and contributes to arterial calcification while elucidating the underlying mechanisms.

Materials and methods

Animal model. The procedures involving Apolipoprotein E knockout ($ApoE^{-/-}$) mice (Beijing Vital River Laboratory Animal Technology Co., Ltd.) were conducted as previously described (21). $ApoE^{-/-}$ mice (8-week-old male) were housed in a controlled facility. Mice were randomly divided into control and high-fat diet (HFD) (n=6 for each group). The control and HFD mice were fed a regular diet and HFD (Dyets, Inc.) for 12 weeks, respectively. $Piezo1^{flox/flox}$ mice were generously provided by Jiaguo Zhou's laboratory (Department of Pharmacology, Cardiac and Cerebral Vascular Research Center, Zhongshan School of Medicine, Sun Yat-Sen University, Guangzhou, China). For the generation of SMC-specific Piezo1 knockout mice, the loxP-Cre system was utilized by administering an adeno-associated virus (AAV) vector expressing Cre recombinase into $Piezo1^{flox/flox}$ mice (described below). $NLRP3^{-/-}$ and $caspase1^{-/-}$ male mice, with a C57BL/6J background, were obtained from ViewSolid Biotech Co., Ltd. and their genotypes were validated through DNA sequencing as previously described (22). $GSDMD^{-/-}$ mice were generously provided by Xun Zhu's laboratory (Department of Microbiology, Zhongshan School of Medicine, Sun Yat-Sen University, Guangzhou, China.). All mice were housed in a specific pathogen-free grade animal laboratory (temperature 20±8˚C, humidity 60±10%, with a 12-h light/dark cycle) and given *ad libitum* access to standard rodent chow and water.

The mice were checked daily for weight, health and behavior. Animals were euthanized if they met the predefined criteria, including rapid weight loss exceeding 15-20% of initial body weight, severe weakness preventing independent access to food or water, prolonged inability to stand (≥24 h) or clinical signs of distress such as marked lethargy and hypothermia (core temperature <37˚C) in the absence of anesthesia. No mice in the present study required euthanasia due to reaching these endpoints, as all maintained stable health throughout the experimental period. Euthanasia was conducted using CO_2 at 30-70% vol/min displacement in compliance with the AVMA guidelines: 2020 Edition (23). The mice were confirmed to be dead when the absence of a heartbeat, pulse, breathing and corneal reflex was observed for >3 min. The animal experiments adhered to ethical standards for animal research and was approved by the Ethics Committee of Zhongshan School of Medicine, Sun Yat-sen University (Guangzhou, China).

AAV construction and administration. The AAV vectors carrying Cre and the negative control were constructed and packaged by HanBio Biotechnology Co., Ltd. Briefly, the pHBAAV-SM22a vector was selected for the present study and the restriction enzymes, *Bam*HI and *Hind*III, were used to cleave the vector, yielding a purified linearized construct. Mouse Cre fragments were amplified using the 2X Flash PCR MasterMix (Dye) kit (CWbio), following the manufacturer's protocol. The HB Infusion™ kit (Hanbio Biotechnology Co., Ltd.) was then employed for the ligation of the linearized vector and mouse Cre fragments, according to the manufacturer's instructions, followed by the transformation of DH5α competent cells (Tiangen Biotech Co., Ltd.). After cultivation in LB medium (Shanghai Yeasen Biotechnology Co., Ltd.) for 12-16 h (selected by antibiotic resistance selection using 100 μg/ml ampicillin), the bacterial cultures were subjected to PCR identification using the 2X Hieff PCR Master Mix (Dye) kit (Shanghai Yeasen Biotechnology Co., Ltd.). The amplified sequence was verified by Sanger sequencing to ensure consistency with Cre.

The plasmid was extracted using the TIANpure Mini Plasmid Kit (Tiangen Biotech Co., Ltd.), and subsequently co-transfected with packaging plasmids (pAAV-RC and pHelper) into 293T cells (Hanbio Biotechnology Co., Ltd.) using Lipofiter™ transfection reagent (HanBio Biotechnology Co., Ltd.). The transfection complex was prepared by mixing the following components: pAAV-RC plasmid 10 μg, pHelper

plasmid 20 μg, Shuttle plasmid 10 μg and Lipofiter 120 μl. The transfection complex was added to the cell culture medium at room temperature. Following 72 h of transfection at 37˚C with 5% CO_2, the 293T cells were harvested, lysed using RIPA (Beyotime Institute of Biotechnology) and centrifuged at 4˚C for 30 min (3,000 x g), with the supernatant collected for virus purification using the ViraTrap™ AAV Purification Maxiprep Kit (Biomiga, Inc.). The resulting viral titer was $1.6x10^{12}$ vg/ml. For gene delivery of Cre specifically to SMCs, the AAV was administered via direct microinjection into the tail vein ($1x10^{11}$ vg per mouse).

Mice and cell calcification construction. A total of 18 healthy Piezo1$^{flox/flox}$ male mice were randomly divided into three experimental groups (n=6/group): Normal diet, high-adenine diet (HAD) + AAV-vector and HAD + AAV-SM22a-cre. The normal diet group received a standard pellet chow diet, while the HAD + AAV-vector group was fed a HAD (0.25% adenine and 1.2% phosphorus) after AAV-vector injection for 4 weeks. The HAD + AAV-SM22a-cre group also received HAD following AAV-SM22a-cre injection for 4 weeks. After 12 weeks of receiving the normal or special diet, the animals were sacrificed. Western blot analysis was performed to validate the efficiency of SMC-specific Piezo1 knockout.

The mice were checked daily for weight, health and behavior. Animals were euthanized if they met the predefined criteria, including rapid weight loss exceeding 15-20% of initial body weight, severe weakness preventing independent access to food or water, prolonged inability to stand (≥24 h) or clinical signs of distress such as marked lethargy and hypothermia (core temperature <37˚C) in the absence of anesthesia. No mice in the present study required euthanasia due to reaching these endpoints, as all maintained stable health throughout the experimental period. Euthanasia was conducted using CO_2 at 30-70% vol/min displacement in compliance with the AVMA guidelines: 2020 Edition (23). The mice were confirmed to be dead when the absence of a heartbeat, pulse, breathing and corneal reflex was observed for >3 min, then the peripheral venous blood and aorta tissues were harvested.

Primary VSMCs were isolated from C57BL/6J mice (8 weeks, 20-25 g, male, n=6/group; Laboratory Animal Center, Sun Yat-sen University), as previously described (24). In brief, after sacrificing the mice (as aforementioned), the thoracic and abdominal aortas were dissected, minced and digested with collagenase (2 mg/ml) for 4 h. The VSMCs were then cultured in Ham's F12 nutrient medium (Gibco; Thermo Fisher Scientific, Inc.) containing 7.5% FBS (Gibco; Thermo Fisher Scientific, Inc.), 100 U/ml penicillin, 100 μg/ml streptomycin and 2 mmol/l L-glutamine at 37˚C with 5% CO_2. First-passage (P1) cells was used in subsequent cell experiments. Human aortic SMCs (HASMCs) were kindly provided by Professor Zhihan Tang's lab (Department of Pathophysiology, Institute of Cardiovascular Disease, Key Laboratory for Arteriosclerology of Hunan Province, University of South China, Hengyang, China) and were cultured in Ham's F12 nutrient medium supplemented with 7.5% FBS at 37˚C under 5% CO_2 (24). For the calcification model, VSMCs at 60% confluency were incubated in a calcifying medium (CM; containing 3.5 mM inorganic phosphate and 3 mM calcium) for 7 days, with comparisons made to VSMCs in growth medium (GM). SMCs at passages 3 to 8 were used for the experiments.

VSMCs were stimulated with oxidized low-density lipoprotein (oxLDL; Guangzhou Yiyuan Biotechnology Co., Ltd.) at varying concentrations (25, 50 and 100 μg/ml), with untreated cells serving as the blank control. After 24 h, cell lysates were collected for subsequent analysis. To assess the impact of NLRP3 inhibition by MCC950 (Selleck Chemicals) on CM-induced calcification, cells were divided into four groups: Control (GM), CM, CM + MCC950 (CM + 100 μM MCC950) and MCC950 (GM + 100 μM MCC950). Similarly, the role of CaMKII inhibition by KN93 (Selleck Chemicals) in CM-triggered pyroptosis was examined using three groups: Control (GM), CM, and CM + KN93 (CM + 10 μM KN93). After 7 days, cell lysates were harvested for further analysis.

Piezo1 differential analysis using gene expression omnibus (GEO) data. Data of the differential expression of Piezo1 (NCBI GEO datasets portal: http://www.ncbi.nlm.nih.gov/geo/; GEO accession no. GSE43292) between macroscopically intact tissue and atheroma plaque was analyzed. The mRNA from microarray analysis had been submitted by Ayari and Bricca (25). Data analysis was performed using GraphPad Prism 6.02 (Dotmatics).

Aortic ring culture. Thoracic to iliac aortas were aseptically excised from male wild type (n=6) and knockout mice (NLRP3$^{-/-}$, caspase1$^{-/-}$ or GSDMD$^{-/-}$) (8 weeks, 20-25 g, n=6/group). After meticulous removal of the adventitia and endothelium, the vessels were segmented into 2-3 mm rings. These segments were then cultured for 7 days at 37˚C under 5% CO_2, with media refreshed every 48 h, using either the calcification medium or standard culture medium. The organ culture experiments were replicated three times under identical conditions.

Antibodies and reagents. The primary antibodies employed in the experiments included anti-Piezo1 (Proteintech Group, Inc.; cat. no. 15939-1-AP; 1:1,000), anti-α smooth muscle actin (α-SMA; Cell Signaling Technology, Inc.; cat. no. 19245s; 1:2,000), anti-alkaline phosphatase (ALP; Novus Biologicals, LLC; Bio-Techne; cat. no. NBP2-67295; 1:2,000), anti-BMP2 (Novus Biologicals, LLC; Bio-Techne; cat. no. NBP1-19751; 1:2,000), anti-RUNX2 (Cell Signaling Technology, Inc.; cat. no. 8486s; 1:2,000), anti-β-actin (Cell Signaling Technology, Inc.; cat. no. 3700S; 1:5,000), anti-NLRP3 (Adipogen Life Sciences; cat. no. AG-20B-0014-C100; 1:2,000), anti-caspase1 (Abclonal Biotech Co., Ltd.; cat. no. A0964; 1:2,000), anti-caspase1 p20 (Biorbyt, Ltd.; cat. no. orb221355; 1:2,000), anti-GSDMD (ImmunoWay Biotechnology Company; cat. no. YT7991; 1:2,000), anti-pro-IL-1β (ImmunoWay Biotechnology Company; cat. no. YM8498; 1:2,000), anti-IL-1β (ImmunoWay Biotechnology Company; cat. no. YT5201; 1:2,000) and anti-CaMKIIδ (Abcam; cat. no. ab181052; 1:2,000). Secondary antibodies used for western blotting included HRP-conjugated goat anti-mouse IgG (H+L) (Cell Signaling Technology, Inc.; cat. no. 7076s; 1:5,000) and HRP-conjugated goat anti-rabbit IgG (H+L) (Cell Signaling Technology, Inc.; cat. no. 7074s; 1:5,000). For immunofluorescence, Alexa Fluor 488-conjugated goat

anti-rabbit IgG (Abcam; cat. no. ab150077; 1:50) and Alexa Fluor 647-conjugated goat anti-mouse IgG (Abcam; cat. no. ab150115; 1:50), GsMTx4 (Abcam; cat. no. ab141871) and Yoda1 (Sigma-Aldrich; Merck KGaA; cat. no. SML1558) were used.

Mouse echocardiography. Echocardiography was performed prior to sacrifice while the mice were anesthetized with isoflurane (induction, 3%; maintenance, 1.5%). Data were collected using the Vivo 2100 imaging system (FUJIFILM VisualSonics, Inc.), as described previously (26). Measurements of wall thickness and lumen diameter were obtained using the system's dedicated software.

Small interfering RNA (siRNA) transfection. siRNA transfection was performed when cells reached 80% confluency, employing the riboFECT™ CP Transfection Kit (Guangzhou RiboBio Co., Ltd.) according to the manufacturer's protocol. For Piezo1 knockdown, VSMCs were treated with siRNA against mouse Piezo1 (siPiezo1). The sequence of siPiezo1 was as follows: 5'-UACCGAUCUCCAGAGACCAUGAUUA-3' for the sense strand, and 5'-UAAUCAUGGUCUGUGGAG AUCGGUU-3' for the antisense strand. The sequence of the control siRNA was as follows: 5'-UUCUCCGAACGUGUC ACGU-3' for the sense strand, and 3'-DTDTAAGAGGCU UGCACAGUGCA-5' for the antisense strand. A 10 μl aliquot of 50 μM siPIEZO1 (Thermo Fisher Scientific, Inc.) or negative control was combined with 120 μl of 1X riboFECT CP buffer, followed by the addition of 12 μl riboFECT CP reagent. After brief vortexing, the solution was maintained at 23˚C for 15 min. Culture medium was then added to the prepared complex to achieve a 2 ml final volume at room temperature, before application to the plated cells. After 48 h of transfection, western blot analysis was performed to validate the efficiency of Piezo1 knockdown.

Western blotting. Protein expression was determined by western blotting as previously described (22). In brief, total protein was extracted from treated cells using RIPA buffer supplemented with a protease inhibitor cocktail and quantified using the BCA Protein Assay Kit (Thermo Fisher Scientific, Inc.). After separating 40 μg of protein per lane by 10% sodium dodecyl sulfate-polyacrylamide gel electrophoresis (SDS-PAGE), the proteins were transferred to polyvinylidene fluoride membranes and blocked with 5% skim milk at room temperature for 2 h. Membranes were incubated overnight at 4˚C with primary antibodies, followed by a 2-h incubation with secondary antibodies at room temperature. Bound proteins were visualized using ECL (MilliporeSigma) and detected on the Bio-Rad ChemiDoc XRS+ chemiluminescent imaging system. Relative protein levels were normalized to β-actin as a loading control and quantified using ImageJ 1.52a software (National Institutes of Health).

Measurement of mitochondrial membrane potential (MMP). The MMP was assessed using JC-1 staining following the manufacturer's protocol. Briefly, cells were incubated in fresh culture medium containing JC-1 dye (Beyotime Institute of Biotechnology) for 30 min at 37˚C in the dark. After two washes with phosphate-buffered saline (PBS), a confocal laser scanning microscope (LSM780; Zeiss GmbH) was used to immediately analyze the samples with 490 nm excitation. Green fluorescence, indicating JC-1 monomers, was recorded at 530 nm emission, while red fluorescence, representing JC-1 aggregates, was recorded at 590 nm. The ratio of yellow fluorescence intensity was calculated using ImageJ 1.52a software to assess the results.

Immunofluorescent staining. Immunofluorescence staining was conducted as previously outlined (22). In summary, aortic rings or cells were fixed in 4% paraformaldehyde for 24 h at 4˚C, sectioned into 7 μm cryostat slices or prepared on chamber slides, followed by blocking with 10% FBS at room temperature for 2 h and permeabilization with Triton X-100. The slides were then incubated overnight at 4˚C with primary antibodies against Piezo1 (1:50), NLRP3 (1:50), ASC (1:50) and α-SMA (1:50). After washing with PBS, secondary antibodies were applied for 1 h at room temperature. Finally, the slides were mounted using a DAPI-containing solution and visualized using a confocal laser scanning microscope (LSM780; Zeiss GmbH). Data analysis was performed using ImageJ 1.52a software.

Alizarin Red S and von Kossa staining. Calcium deposition in the aorta and VSMCs was evaluated using Alizarin Red S staining. Aortic rings were fixed in 4% polyoxymethylene for 1 h at room temperature, and cells for 20 min. After two PBS washes, both aortic rings and cells were stained with 1% Alizarin Red solution for 10 min at room temperature, followed by three additional PBS washes before imaging under a light microscope. For von Kossa staining, aortic sections were dewaxed, hydrated and treated with 1% silver nitrate under ultraviolet light for 10 min. Calcified nodules were visualized as brown to black under a light microscope or ELISPOT analyzer (CTL ImmunoSpot® S6 Ultimate) following multiple washes. Data analysis was performed using ImageJ 1.52a software.

Hematoxylin and eosin (H&E) staining. Following a 2-h baking period at 60˚C to ensure tissue adhesion, lesion sections underwent standard H&E staining. Deparaffinization was performed through two 5-min xylene immersions, followed by graded rehydration in absolute ethanol and decreasing ethanol concentrations (95, 80 and 70%, 5 min each) and three 2-min distilled water washes. Nuclear staining was achieved via 5-min hematoxylin incubation, followed by running water rinsing, brief acidic ethanol differentiation and a 5-min water wash. Cytoplasmic staining employed 2-min eosin application with subsequent water rinsing. Dehydration involved sequential 10-sec immersions in 70, 80 and 90% ethanol, 5 min in absolute ethanol and two final 5-min xylene clears before neutral resin mounting. All procedures except the initial baking were conducted at 20-25˚C. Stained sections were examined using an Olympus VS200 automated microscope.

Co-immunoprecipitation (Co-IP). Cells were lysed on ice for 15 min using RIPA buffer containing a protease inhibitor cocktail and PMSF. After centrifugation at 14,000 x g (15 min, 4˚C), the resulting 40 μg supernatant was

subjected to co-immunoprecipitation with an anti-CaMKIIδ (GeneTex, Inc.; cat. no. GTX111401; 1:100) or anti-RUNX2 antibody (Abcam; cat. no. ab236639; 1:100) or anti-rabbit IgG (Proteintech Group, Inc.; cat. no. SA00001-2; 1:1,000) overnight at 4˚C. Protein A-conjugated agarose beads (MilliporeSigma; cat. no. IP05; 40 μl) were then introduced, followed by a 1-h incubation at 4˚C with rotation. The beads underwent six washes with chilled lysis buffer before resuspension in SDS-PAGE loading buffer. Bound proteins were eluted by heating at 92˚C for 3 min and separated on a 10% polyacrylamide gel via SDS-PAGE. Finally, CaMKII and RUNX2 levels were detected by immunoblotting as previously described.

Terminal deoxynucleotidyl transferase-mediated dUTP nick-end labeling (TUNEL) staining. Aortic ring sections (7 μm) were fixed in 4% paraformaldehyde 1 h at room temperature and incubated with TUNEL reaction mixture (Beyotime Institute of Biotechnology) at 37˚C for 1 h in a light-protected environment. Nuclear staining was performed using mounting medium with DAPI (Abcam; cat. no. ab1041395) for 10 min at room temperature, ensuring light protection throughout the procedure. A fluorescence microscope (Leica DM6B; Leica Microsystems GmbH) was employed to capture images at various magnifications, and TUNEL-positive cells were counted from three randomly selected fields for each sample.

Statistical analysis. All data are presented as mean ± SD. Each *in vitro* experiment was repeated at least three times. Pearson's correlation analysis coefficient was employed for correlation analysis. Unpaired Student's t-test was used to compare the mean of two groups. For comparisons across multiple groups, one-way ANOVA with the Tukey's multiple comparisons test was applied. Data analysis was performed using GraphPad Prism 6.02 (Dotmatics). $P<0.05$ was considered to indicate a statistically significant difference.

Results

Piezo1 is upregulated in the atherosclerotic plaques of mice and patients. Vascular calcification frequently occurs within atherosclerotic plaques (27). To investigate the role of Piezo1 in this process, Piezo1 expression was examined in ApoE$^{-/-}$ mice subjected to a high-fat diet, which induces atherosclerotic calcification (28). Elevated Piezo1 expression was observed in both the necrotic core of atherosclerotic plaques and the adjacent vascular wall (Fig. 1A). To corroborate this finding in humans, data from the human carotid atheroma dataset (GSE43292) was analyzed, revealing that Piezo1 expression was significantly higher in atherosclerotic plaques compared with macroscopically intact tissue (Fig. 1B). In addition, primary VSMCs from mice were treated with ox-LDL at varying concentrations, resulting in a dose-dependent increase in Piezo1 expression (Fig. 1C). Immunofluorescence staining confirmed that Piezo1 expression was upregulated and primarily localized on the cell membrane (Fig. 1D). These results suggest a potential connection between Piezo1 and the progression of atherosclerosis.

CM-induced osteogenic differentiation is associated with Piezo1 expression, NLRP3 inflammasome activation and pyroptosis in aortic ring and VSMCs. To further elucidate the role of Piezo1 in vascular calcification, aortic rings were cultured in either GM or CM. Exposure to CM over time compromised vascular integrity (Fig. 2A), coinciding with increased Piezo1 expression and decreased α-SMA levels (Fig. 2A-C). Pyroptosis of plaque VSMCs, a known contributor to plaque rupture and instability (29), was examined next. CM-induced osteogenic differentiation in primary VSMCs was demonstrated by increased expression of the osteogenic markers, ALP, BMP2 and RUNX2, alongside elevated Piezo1 levels (Fig. 2D and E). Pyroptotic markers, including cleaved caspase1, cleaved IL-1β and GSDMD-NT, were also upregulated in CM-treated VSMCs (Fig. 2D-F). Notably, Piezo1 expression showed a positive correlation with RUNX2 ($R^2=0.3089$; $P=0.0354$; Fig. 2G) and IL-1β ($R^2=0.7693$; $P=0.0154$; Fig. 2H), suggesting a potential link between Piezo1 and both osteogenic differentiation and inflammation. To further elucidate the mechanisms driving calcification and pyroptosis, mitochondrial function was assessed. CM treatment caused mitochondrial dysfunction in VSMCs, as indicated by a disrupted MMP (Fig. 2I). Additionally, activated NLRP3 inflammasomes, marked by NLRP3-ASC binding, were observed in VSMCs following CM exposure (Fig. 2J). These results indicate that CM promotes Piezo1 expression in a time-dependent manner which may lead to pyroptosis in VSMCs, contributing to vascular calcification.

VSMC-specific knockout of Piezo1 alleviates arterial calcification in mice. To further explore the involvement of Piezo1 in arterial calcification, VSMC-specific Piezo1 knockout mice were generated by administering AAV-SM22α-Cre to Piezo1$^{flox/flox}$ mice, followed by an HAD to induce vascular calcification (Fig. 3A). HAD significantly impaired cardiac function, which was mitigated in the Piezo1 knockout group (Fig. 3B). Moreover, the knockout of Piezo1 in VSMCs attenuated HAD-induced aortic calcification, as demonstrated by M-mode echocardiography of the thoracic and abdominal aorta (Fig. 3C). Alizarin Red staining further confirmed the reduction in HAD-induced calcium deposition in the knockout mice (Fig. 3D and E). Notably, VSMC-specific Piezo1 knockout resulted in increased aortic lumen thickness (Fig. 3F). Collectively, these results suggest that Piezo1 deficiency in VSMCs inhibits arterial calcification and improves cardiac function.

Piezo1 inhibition blocks CM-induced NLRP3 inflammasome activation and pyroptosis and alleviates calcification. Von Kossa staining showed that CM-induced vascular calcification and structural damage in cultured aortic rings, which was alleviated by the Piezo1-specific inhibitor, GsMTx4 (5 μM) (Fig. 4A and B). Given the role of VSMC death in vascular calcification (30), TUNEL staining was performed to assess cell death in the cultured cells. Calcifying conditions significantly increased cell death, which was reduced by GsMTx4 (Fig. 4C and D). Alizarin Red S staining also confirmed that Piezo1 inhibition reduced calcium deposition in VSMCs (Fig. 4E and F). Moreover, CM treatment led to increased expression of the osteogenic markers, ALP, BMP2

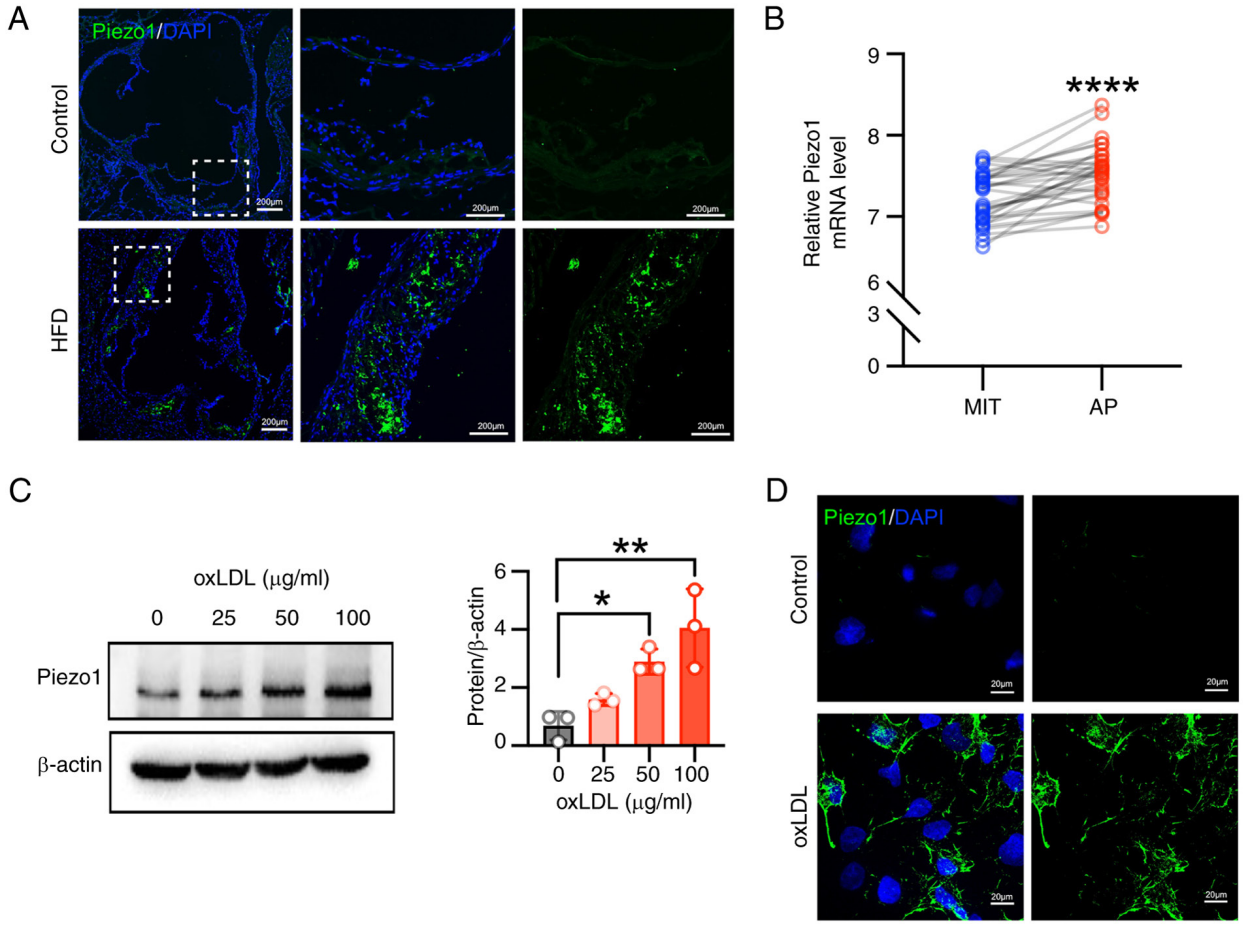

Figure 1. Piezo1 is upregulated in atherosclerosis plaques in both patients and mice. (A) Representative immunofluorescence stained images of aortic tissues isolated from Apolipoprotein E$^{-/-}$ mice (scale bars, 200 μm). Piezo1 is shown in green and DAPI is shown in blue; n=6 rats per group. (B) Relative mRNA expression of Piezo1 in human carotid samples (data from GEO dataset, GSE43292; paired t-test; n=32); ****P<0.0001 vs. MIT. Statistical significance of mRNA expression was assessed by paired Student's t-test (C) VSMCs were treated with oxLDL for 24 h, and Piezo1 protein expression was determined by western blot; *P<0.05, **P<0.01 vs. control. Statistical significance was assessed by one-way ANOVA followed by Tukey's. (D) Representative immunofluorescence stained images of Piezo1 (green) in VSMCs (scar bar, 20 μm). Cell nuclei were counterstained with DAPI (blue). All values are presented as mean ± SD. AP, atheroma plaque; MIT, macroscopically intact tissue; oxLDL, oxidized low-density lipoprotein; HFD, high-fat diet; VSMCs, vascular smooth muscle cells.

and RUNX2, which were significantly inhibited by either Piezo1 inhibitor or Piezo1 siRNA (Fig. 4G-J). Similarly, CM-induced activation of the NLRP3 inflammasome and pyroptosis in VSMCs was blocked by Piezo1 inhibition or knockdown (Fig. 4G-I). These results confirm that Piezo1 plays a key role in VSMC osteogenic differentiation, with its effects closely linked to NLRP3 inflammasome activation and pyroptosis.

Piezo1 activator promotes CM-induced NLRP3 inflammasome activation and pyroptosis and enhances calcification. To further clarify the role of Piezo1 in the osteogenic differentiation of VSMCs, Piezo1 was activated using Yoda1 (30 μM), which enhanced calcium deposition. Yoda1 significantly promoted CM-induced calcium deposits in aortic rings (Fig. 5A and B). Additionally, calcifying conditions increased cell death, which was exacerbated by Yoda1 (Fig. 5C and D). Alizarin Red S staining confirmed that Yoda1 further enhanced CM-induced calcium deposition in VSMCs (Fig. 5E and F). Consistently, Yoda1 increased the expression of the osteogenic markers, ALP and BMP2, and promoted NLRP3 inflammasome activation and pyroptosis (Fig. 5G-I). These results further demonstrate that Piezo1 may be a critical modulator of VSMC osteogenic differentiation and vascular calcification, with its activity being associated with inflammasome activation and pyroptosis.

NLRP3, caspase1 or GSDMD deletion inhibits CM-induced calcification with/without Piezo1 agonist. To investigate the specific role of NLRP3 inflammasome activation and pyroptosis in arterial calcification, aortic rings from NLRP3$^{-/-}$, caspase1$^{-/-}$ and GSDMD$^{-/-}$ mice were treated with CM in the presence or absence of the Piezo1 activator, Yoda1. Notably, CM-induced arterial calcification was significantly suppressed by the deletion of NLRP3, caspase1 or GSDMD, even when Yoda1 was present in the medium (Fig. 6A and B). TUNEL staining also revealed that the deletion of these genes reduced cell death in CM-cultured aortic rings, despite Yoda1 treatment (Fig. 6C and D). Moreover, the NLRP3-specific inhibitor, MCC950, effectively blocked CM-induced calcium nodule formation and calcium deposition in VSMCs (Fig. 6E and F). These results suggest that NLRP3 inflammasome activation and pyroptosis may be key contributors to Piezo1-mediated arterial calcification.

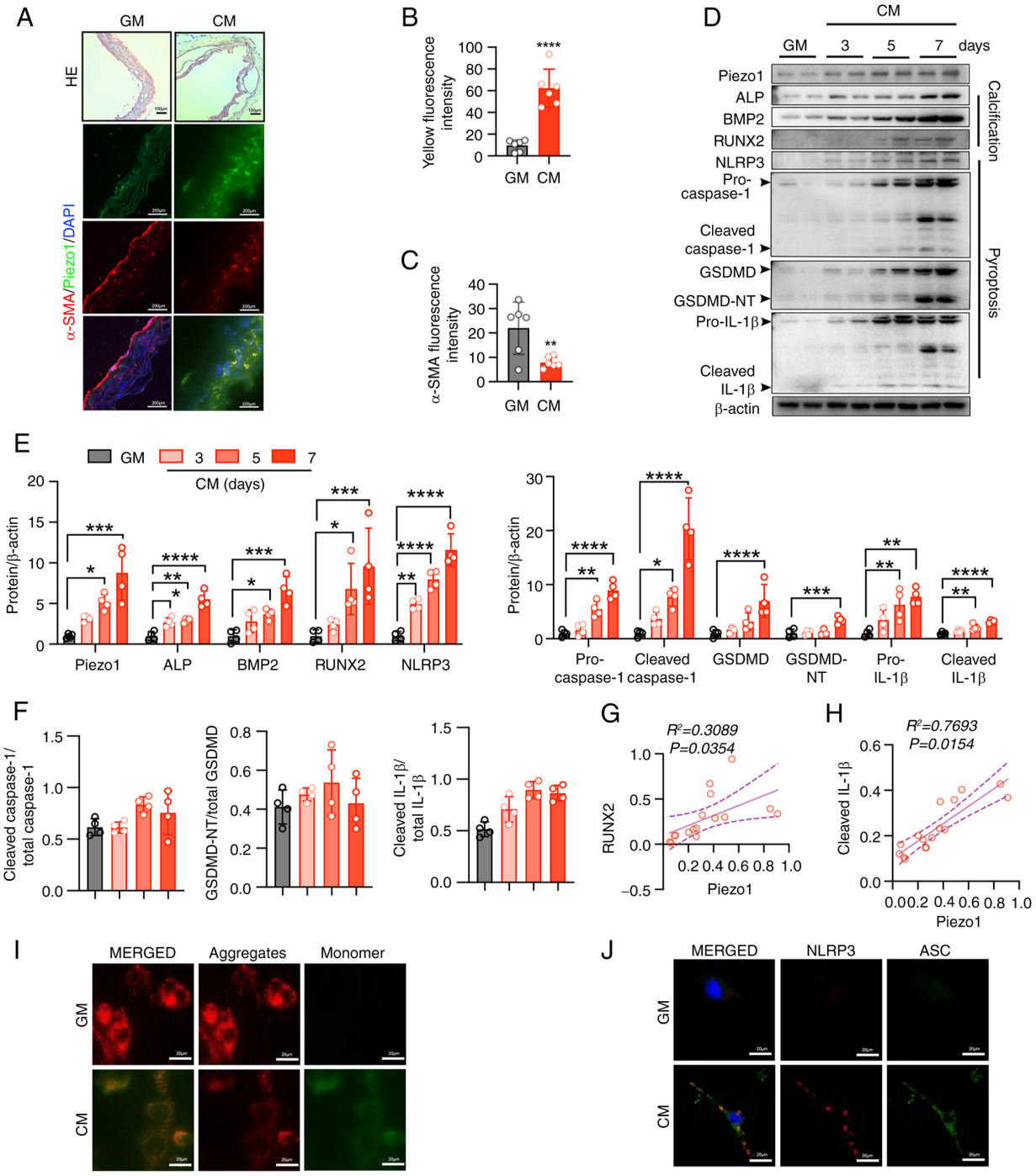

Figure 2. CM-induced osteogenic differentiation is associated with Piezo1 expression, NLRP3 inflammasome activation and pyroptosis in the aortic ring and VSMCs. (A) Representative H&E staining and immunofluorescence images alongside (B and C) quantification of α-SMA and Piezo1 expression in the aortic sections of mice (HE scale bars, 100 μm; immunofluorescence scale bars, 200 μm); ****P<0.0001 vs. GM. Statistical significance of mRNA expression was assessed by unpaired Student's t-test (D-F) Representative immunoblot images and semi-quantification of Piezo1, ALP, BMP2, RUNX2, NLRP3, pro-caspase1, cleaved-caspase1, GSDMD, GSDMD-NT, pro-IL-1β, cleaved-IL-1β, cleaved caspase1/total-caspase1, GSDMD-NT/total GSDMD and cleaved IL-1β/total IL-1β in mouse VSMC extracts. β-actin was used as a loading control; *P<0.05, **P<0.01, ***P<0.001, ****P<0.0001 vs. GM. Statistical significance was assessed by one-way ANOVA followed by Tukey's. Correlation analysis between Piezo1 protein expression and the (G) RUNX2 and (H) IL-1β level. Pearson's correlation analysis coefficient was employed for correlation analysis. (I) MMP changes were monitored by fluorescence using JC-1 staining. (J) Representative immunofluorescence images of inflammasome marker NLRP3 and ASC expression in the VSMCs of mice. Scale bars, 10 μm; n=3 independent experiments; ***P<0.001 vs. GM. All values are presented as mean ± SD. CM, calcifying medium; GM, growth medium; NLRP3, NOD-like receptor thermal protein domain-containing protein 3; VSMCs, vascular smooth muscle cells; α-SMA, α-smooth muscle actin; ALP, alkaline phosphatase; BMP2, bone morphogenetic protein 2; RUNX2, runt-related transcription factor 2; GSDMD, gasdermin D; GSDMD-NT, gasdermin D N-terminal; IL-1β, interleukin-1β; MMP, mitochondrial membrane potential; ASC, apoptosis-associated speck-like protein containing a caspase recruitment domain.

CaMKII promotes CM-induced calcium deposits via binding to RUNX2 in VSMCs. To further explore the downstream mechanisms of Piezo1 in arterial calcification, the interaction between Piezo1 and transcription factors involved in osteoblast mineralization was examined. It has been reported that Ca^{2+}/calmodulin signaling regulates RUNX2 activity,

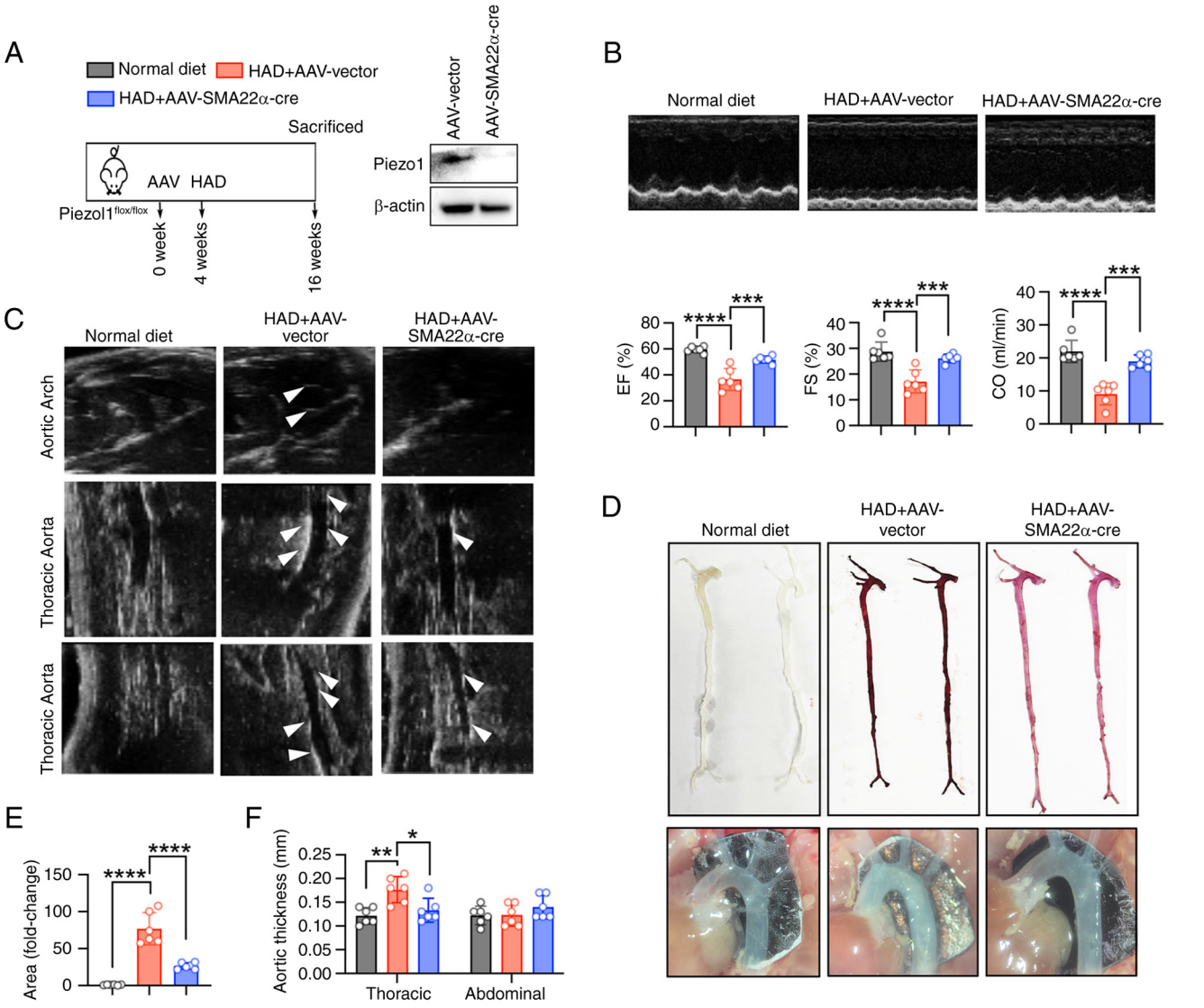

Figure 3. Specific knockout of Piezo1 in VSMCs alleviates arterial calcification in mice. (A) Schematic representation of the arterial calcification *in vivo* protocol. (B) Representative echocardiographic recordings revealed that HAD induced cardiac dysfunction in VSMC-specific Piezo1 knockout mice (generated via AAV-SMA22α-cre). Cardiac dysfunction was evaluated using echocardiographic parameters including EF, FS and CO; ***P<0.001, ****P<0.0001. (C) Representative 2D B-mode images from the *in vivo* ultrasound scanning of the aortic arch, thoracic aorta and abdominal aorta. White arrows indicate vascular calcifications. (D and E) Representative images of Alizarin red staining revealed that a HAD-induced calcium deposition in the aorta (reddish signal) of VSMC-specific Piezo1 knockout mice. The whole-aorta analysis further confirmed calcification extent; ****P<0.0001. (F) Recorded aortic thickness; *P<0.05, **P<0.01. Statistical significance was assessed by one-way ANOVA followed by Tukey's. All values are presented as mean ± SD. AAV, adeno-associated virus; HAD, high-adenine diet; w, weeks; EF, ejection fraction; FS, fraction shortening; CO, cardiac output; VSMC, vascular smooth muscle cells.

a critical mediator in osteoblast differentiation (31,32), suggesting a Ca^{2+}-dependent regulatory pathway in vascular calcification. Hence, the interaction between CaMKII and RUNX2 in Piezo1-mediated VSMC osteogenic transition was investigated in the present study. Immunoprecipitation confirmed that CaMKII directly interacts with RUNX2 (Fig. 7A and B), and immunofluorescence demonstrated that CM treatment promoted the co-localization of CaMKII and RUNX2 in VSMCs (Fig. 7C). Alizarin Red S staining also showed that KN93 reduced CM-induced calcium nodule formation and calcium deposition in VSMCs (Fig. 7D). Furthermore, inhibition of CaMKII with KN93 significantly alleviated CM-induced pyroptosis and the expression of osteogenic markers in VSMCs (Fig. 7E-G). These results suggest that activated CaMKII binding to RUNX2 may play a pivotal role in modulating VSMC differentiation into osteoblast-like cells.

Piezo1 inhibition alleviates HASMC differentiation into osteoblasts. Consistent with the findings in VSMCs, CM treatment also increased Piezo1 expression, activated the NLRP3 inflammasome and induced pyroptosis in HASMCs (Fig. 8A and C-E). In parallel, CM-treated HASMCs exhibited significantly elevated expression of the osteoblast differentiation markers, ALP, BMP2 and RUNX2 (Fig. 8C and D). Notably, these effects were significantly inhibited by the Piezo1 inhibitor, GsMTx4 (Fig. 8C-E). Alizarin Red S staining further confirmed that Piezo1 inhibition abolished CM-induced calcium nodule formation and calcium deposition in HASMCs (Fig. 8B). Collectively, these results confirm

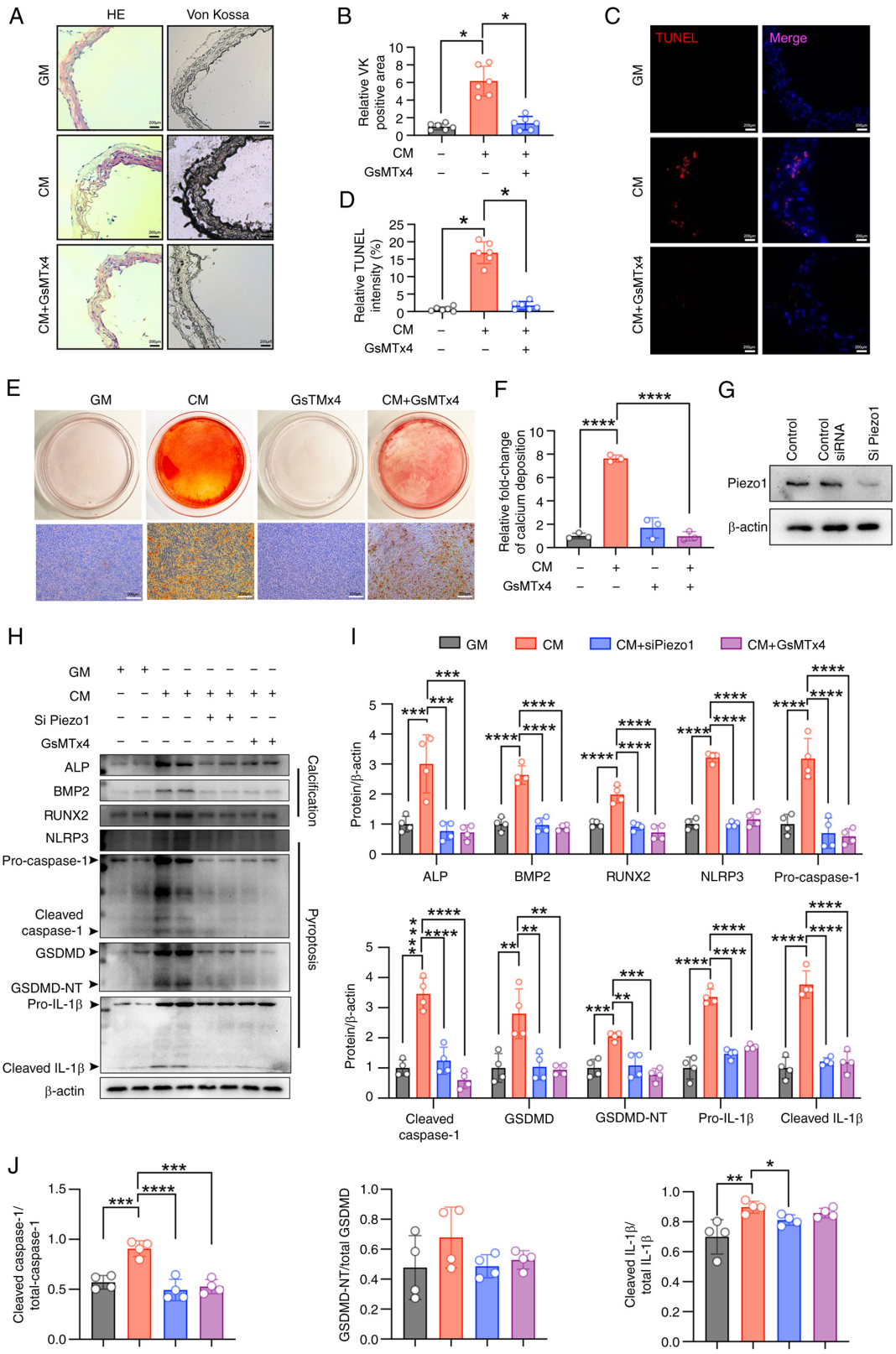

Figure 4. Piezo1 inhibition blocks CM-induced NLRP3 inflammasome activation and pyroptosis and alleviates calcification. (A and B) Representative HE staining, Von Kossa staining and quantification of the Von Kossa positive area in the aortic sections of mice (scale bars, 200 μm); *P<0.05. (C and D) TUNEL staining analysis was used to evaluate cell death (scale bars, 200 μm); *P<0.05. (E and F) Representative images of Alizarin red S staining showing calcium nodule formation (reddish signal) in VSMCs cultured with GM/CM under Piezo1 inhibitor treatment (scale bars, 200 μm); ****P<0.0001; n=3 independent experiments. (G-J) Representative immunoblot images of Piezo1, ALP, BMP2, RUNX2, NLRP3, pro-caspase1, cleaved-caspase1, GSDMD, GSDMD-NT, pro-IL-1β, cleaved-IL-1β, cleaved caspase1/total-caspase1, GSDMD-NT/total GSDMD and cleaved IL-1β/total IL-1β in mouse VSMC extracts. β-actin was used as a loading control. **P<0.01, ***P<0.001, ****P<0.0001. Statistical significance was assessed by one-way ANOVA followed by Tukey's. All values are presented as mean ± SD. CM, calcifying medium; GM, growth medium; VK, von kossa; TUNEL, terminal deoxynucleotidyl transferase-mediated dUTP nick-end labeling; VSMCs, vascular smooth muscle cells; ALP, alkaline phosphatase; BMP2, bone morphogenetic protein 2; RUNX2, runt-related transcription factor 2; NLRP3, NOD-like receptor thermal protein domain-containing protein 3; GSDMD, gasdermin D; GSDMD-NT, gasdermin D N-terminal; IL-1β, interleukin-1β; siRNA, small interfering RNA.

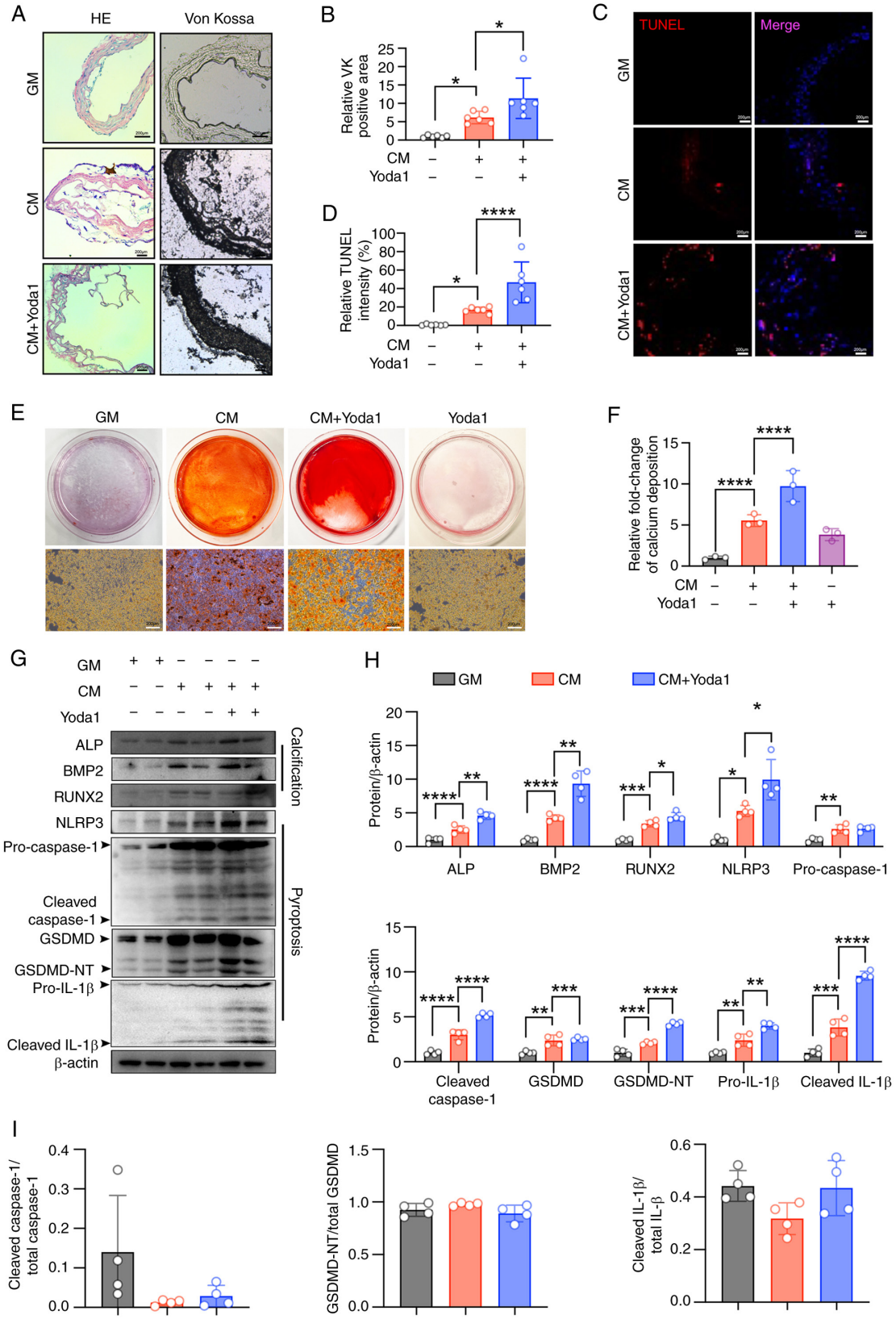

Figure 5. Piezo1 activator promotes CM-induced NLRP3 inflammasome activation and pyroptosis and enhances calcification. (A and B) Representative HE staining, Von Kossa staining and quantification of the Von Kossa positive area in the aortic sections of mice (scale bars, 200 μm); *P<0.05. (C and D) TUNEL staining analysis was used to evaluate cell death (scale bars, 200 μm); *P<0.05, ****P<0.0001. (E and F) Calcium deposition was visualized by Alizarin red S staining at the light microscopic level (scale bars, 200 μm); ****P<0.0001; n=3 independent experiments. (G-I) Representative immunoblot images of Piezo1, ALP, BMP2, RUNX2, NLRP3, pro-caspase1, cleaved-caspase1, GSDMD, GSDMD-NT, pro-IL-1β, cleaved-IL-1β, cleaved caspase1/total-caspase1, GSDMD-NT/total GSDMD and cleaved IL-1β/total IL-1β in mouse VSMC extracts. β-actin was used as a loading control. *P<0.05, **P<0.01, ***P<0.001, ****P<0.0001. Statistical significance was assessed by one-way ANOVA followed by Tukey's. All values are presented as mean ± SD. CM, calcifying medium; GM, growth medium; VK, von kossa; TUNEL, terminal deoxynucleotidyl transferase-mediated dUTP nick-end labeling; ALP, alkaline phosphatase; BMP2, bone morphogenetic protein 2; RUNX2, runt-related transcription factor 2; NLRP3, NOD-like receptor thermal protein domain-containing protein 3; GSDMD, gasdermin D; GSDMD-NT, gasdermin D N-terminal; IL-1β, interleukin-1β; VSMC, vascular smooth muscle cells.

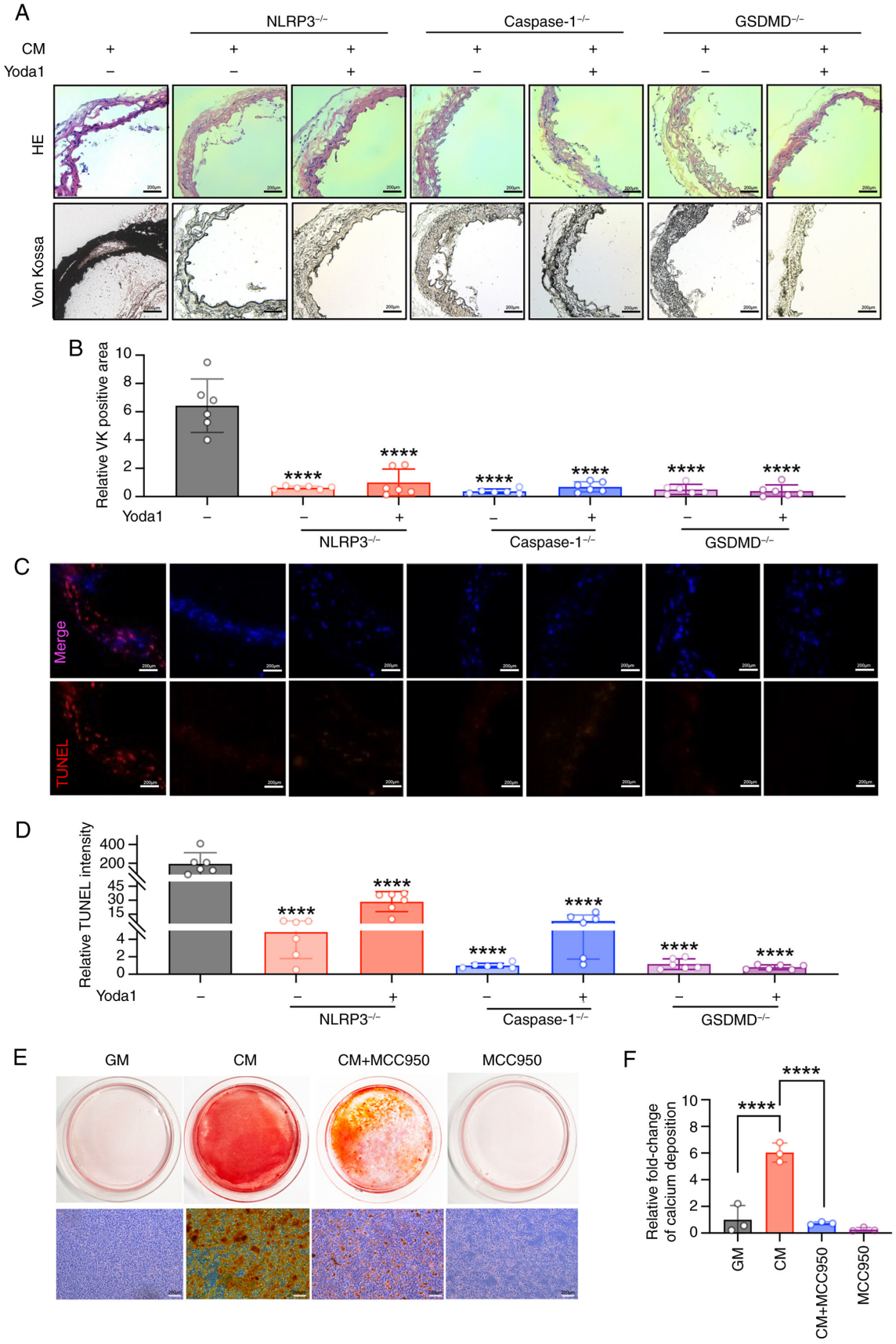

Figure 6. NLRP3, caspase1 or GSDMD deletion inhibits CM-induced calcification with/without Piezo1 agonist. (A and B) Representative HE staining, Von Kossa staining and quantification of the Von Kossa positive area in the aortic sections of NLRP3$^{-/-}$, caspase1$^{-/-}$ and GSDMD$^{-/-}$ mice (scale bars, 200 μm); ****P<0.0001 vs. CM. (C and D) TUNEL staining analysis was used to evaluate cell death (scale bars, 200 μm); ****P<0.0001 vs. CM. (E and F) Calcium deposition in VSMCs was visualized by Alizarin red S staining at the light microscopic level (scale bars, 200 μm); ****P<0.0001. Statistical significance was assessed by one-way ANOVA followed by Tukey's. All values are presented as mean ± SD. CM, calcifying medium; GM, growth medium; VK, von kossa; TUNEL, terminal deoxynucleotidyl transferase-mediated dUTP nick-end labeling; NLRP3, NOD-like receptor thermal protein domain-containing protein 3; GSDMD, gasdermin D; VSMC, vascular smooth muscle cells.

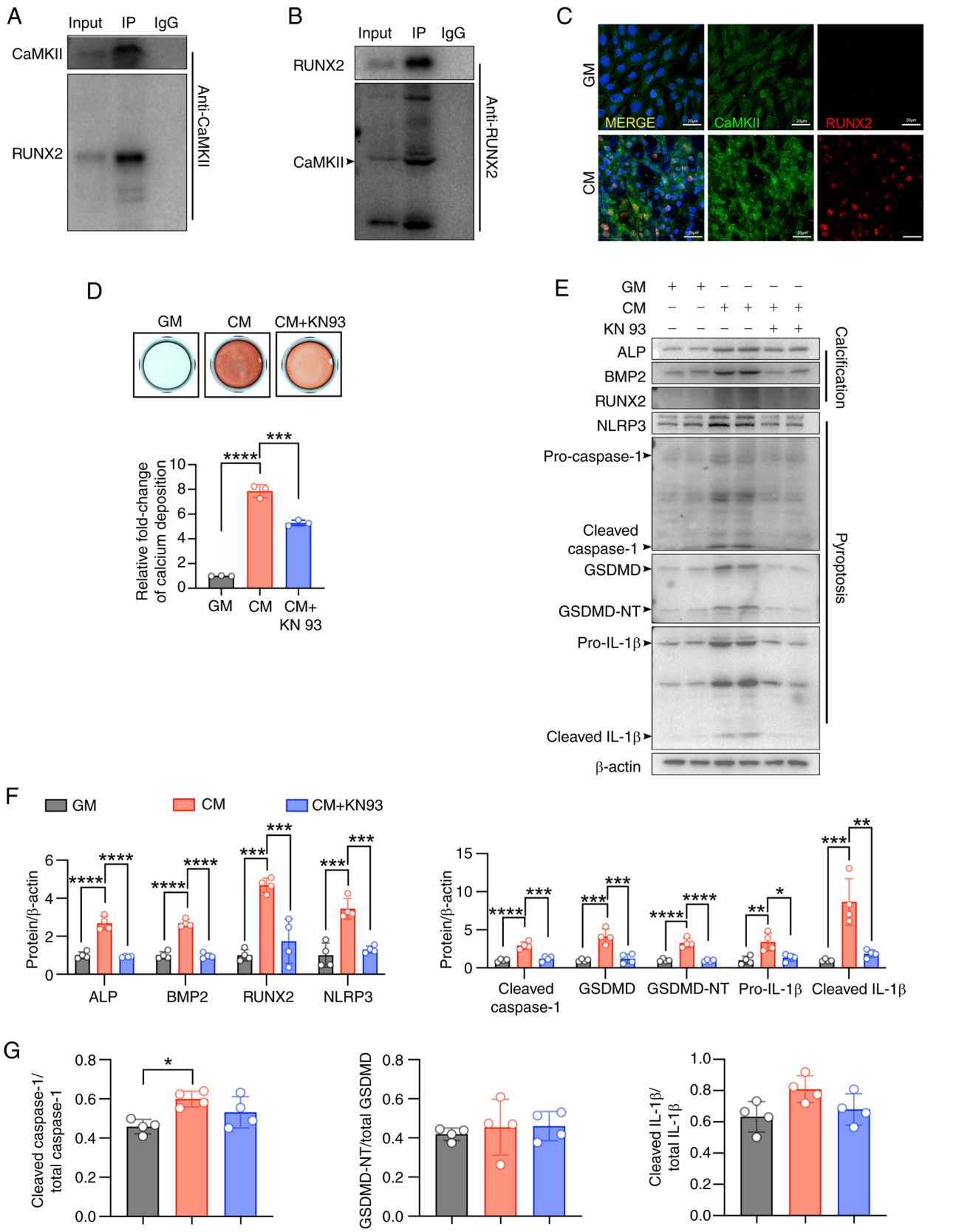

Figure 7. CaMKII promotes CM-induced calcium deposits via binding RUNX2 in VSMCs. (A and B) Co-immunoprecipitation of CaMKII with RUNX2 in VSMCs. (C) Representative immunofluorescence images of CaMKII and RUNX2 in VSMCs (scale bars, 20 μm). (D) Calcium deposition of VSMCs was visualized in 24-well plate by Alizarin red S staining at the light microscopic level; ***P<0.001, ****P<0.0001. (E-G) Representative immunoblot images of Piezo1, ALP, BMP2, RUNX2, NLRP3, pro-caspase1, cleaved-caspase1, GSDMD, GSDMD-NT, pro-IL-1β, cleaved-IL-1β, cleaved caspase1/total-caspase1, GSDMD-NT/total GSDMD and cleaved IL-1β/total IL-1β in mouse VSMC extracts. β-actin was used as a loading control. *P<0.05, **P<0.01, ***P<0.001, ****P<0.0001. Statistical significance was assessed by one-way ANOVA followed by Tukey's. All values are presented as mean ± SD. CM, calcifying medium; GM, growth medium; CaMKII, calcium/calmodulin dependent protein kinase II; VSMCs, vascular smooth muscle cells; IP, immunoprecipitation; ALP, alkaline phosphatase; BMP2, bone morphogenetic protein 2; RUNX2, runt-related transcription factor 2; NLRP3, NOD-like receptor thermal protein domain-containing protein 3; GSDMD, gasdermin D; GSDMD-NT, gasdermin D N-terminal; IL-1β, interleukin-1β.

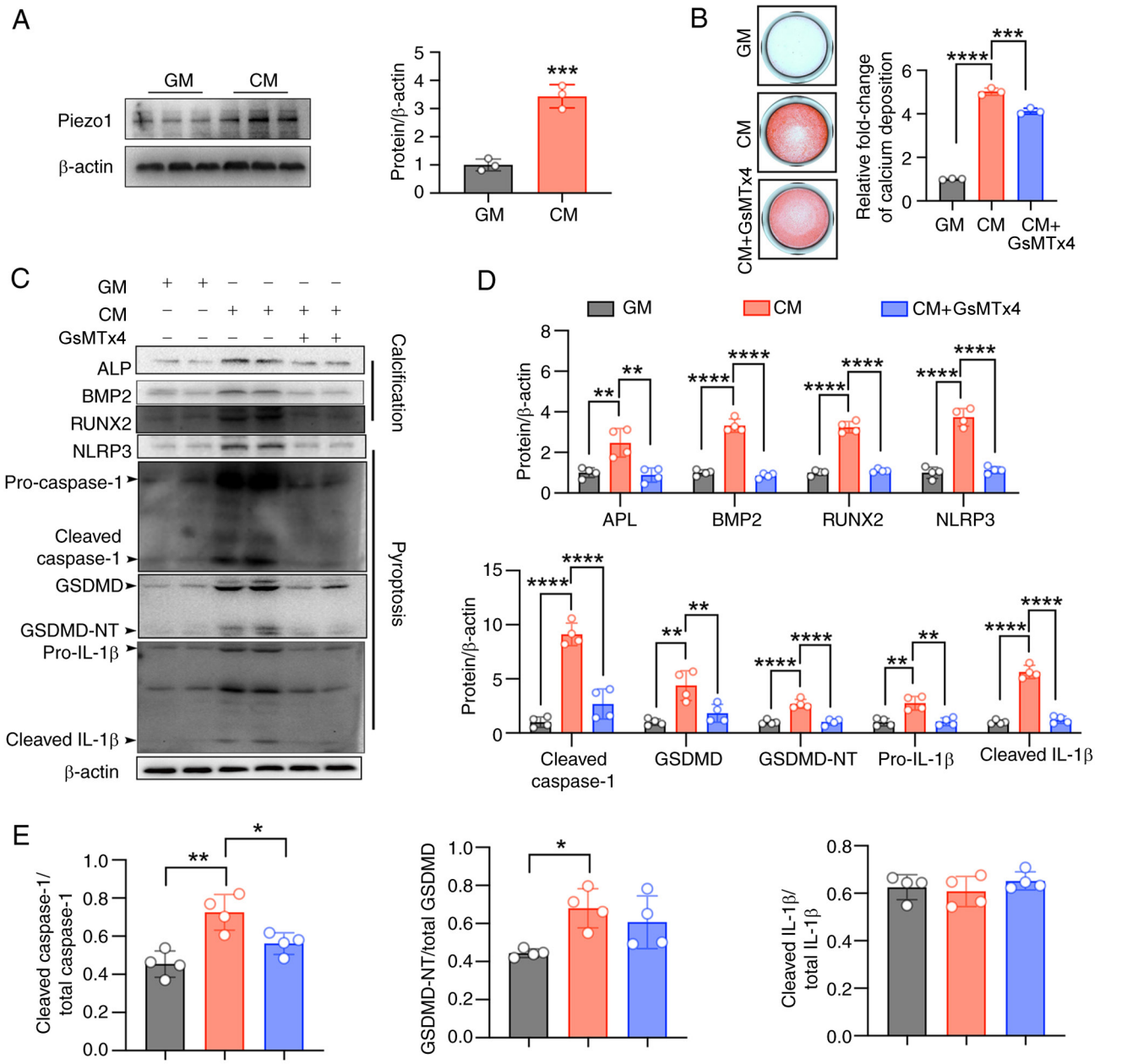

Figure 8. Piezo1 inhibition alleviates HASMC differentiation into osteoblasts. (A) Representative immunoblot images of Piezo1 in HASMC extracts. β-actin was used as a loading control; ***P<0.001. Statistical significance of mRNA expression was assessed by unpaired Student's t-test (B) Calcium deposition of HASMCs was visualized in 24-well plate by Alizarin red S staining at the light microscopic level; ***P<0.001, ****P<0.0001. (C-E) Representative immunoblot images of Piezo1, ALP, BMP2, RUNX2, NLRP3, pro-caspase1, cleaved-caspase1, GSDMD, GSDMD-NT, pro-IL-1β, cleaved-IL-1β, cleaved caspase1/total-caspase1, GSDMD-NT/total GSDMD and cleaved IL-1β/total IL-1β in HASMCs extracts. β-actin was used as a loading control; *P<0.05, **P<0.01, ****P<0.0001. Statistical significance was assessed by one-way ANOVA followed by Tukey's. All values are presented as mean ± SD. HASMC, human aortic smooth muscle cells; CM, calcifying medium; GM, growth medium; ALP, alkaline phosphatase; BMP2, bone morphogenetic protein 2; RUNX2, runt-related transcription factor 2; NLRP3, NOD-like receptor thermal protein domain-containing protein 3; GSDMD, gasdermin D; GSDMD-NT, gasdermin D N-terminal; IL-1β, interleukin-1β.

that Piezo1 activation may promote osteogenic differentiation and calcification in HASMCs through NLRP3 inflammasome activation and pyroptosis.

Discussion

In the present study, the detrimental role of Piezo1 in arterial calcification was identified. To the best of our knowledge, the present study is the first to report that depletion of Piezo1 in VSMCs effectively protected mice from developing arterial calcification. Additionally, *in vitro* experiments demonstrated that Piezo1 activation significantly contributed to IL-1β expression and pro-inflammatory cell death (pyroptosis), which subsequently drove VSMC calcification. Mechanistically, the present study provided the first evidence that the downstream effector of Piezo1, CaMKII, initiated inflammasome assembly and pyroptosis, leading to VSMC calcification. Simultaneously, CaMKII interacted with RUNX2, promoting the expression of osteogenic proteins. These novel findings highlight Piezo1 as a promising therapeutic target for arterial calcification by

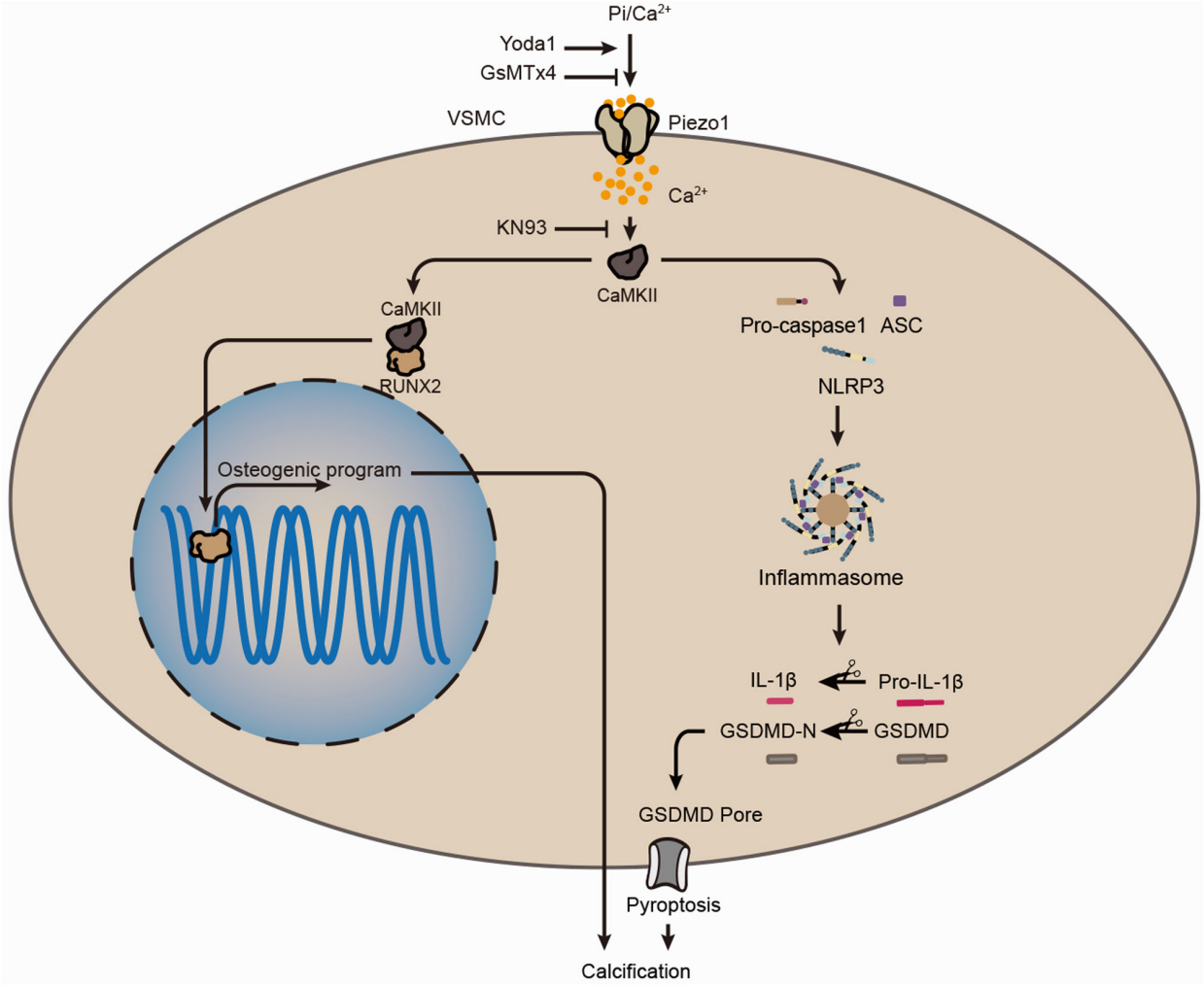

Figure 9. Potential mechanisms by which Piezo1 activation contributes to calcification in VSMCs. Piezo1 promotes vascular calcification by activating Ca^{2+}-CaMKII signaling, which triggers NLRP3 inflammasome formation and induces pyroptosis in VSMCs. VSMCs, vascular smooth muscle cells; CaMKII, calcium/calmodulin dependent protein kinase II; NLRP3, NOD-like receptor thermal protein domain-containing protein 3; ASC, apoptosis-associated speck-like protein containing a caspase recruitment domain; RUNX2, runt-related transcription factor 2; GSDMD, gasdermin D; GSDMD-NT, gasdermin D N-terminal; IL-1β, interleukin-1β.

regulating VSMC pyroptosis. Notably, aberrant Piezo1-induced vascular pyroptosis and calcification were reversed by Piezo1 inhibition, whether through pharmacological or genetic approaches.

It is well-established that shear stress and tissue stiffness are the primary factors driving Piezo1 activation through mechanosensation (33,34). In human fibroatheromas, microcalcifications >5 μm have been shown to increase peak circumferential stress by 2-7 times (35). The present study, along with others, has reported elevated Piezo1 expression in both human and murine atherosclerotic plaques (36) and calcified vessels (37), which leads to vascular inflammation (38). It has been demonstrated that VSMCs in the fibrous caps of microcalcifications undergo calcification via Piezo1 activation in response to mechanical stimuli such as tissue stiffness, shear stress and extracellular pressure (39). Notably, the results of the present study also revealed that Piezo1 could be activated independently of mechanical forces, with elevated expression observed under high calcium/phosphate conditions.

The findings of the present study, alongside previous research, underscore the role of ion channels in the osteogenic transition of VSMCs and arterial calcification (40,41). In the present study, it was observed that CM induced Piezo1 upregulation and calcification in a time-dependent manner, with CM-induced calcification showing a synergistic effect with Piezo1 activation. This synergistic interaction, supported by the increased expression of osteogenic markers and a previous study (37), helps to explain the strong correlation between pulse pressure, isolated systolic hypertension and calcified atherosclerosis (42). Thus, Piezo1 activation is essential for arterial calcification.

Previous studies have demonstrated that Piezo1-mediated processes, such as cell death and division, play critical roles in biological functions and disease progression (17,43,44). To the best of our knowledge, the present study is the first to reveal that Piezo1 activation induces pyroptosis in VSMCs and drives inflammasome activation during CM-induced cell death and osteogenic differentiation. Piezo1-induced inflammasome assembly appears to function in parallel with the canonical pathway, in which NLRs and AIM2-like receptors detect pathogen-associated molecular patterns and DAMPs, triggering the assembly of a caspase1-activating complex (45). In

line with the established role of Piezo1 as a calcium-dependent mechanotransducer (46), Piezo1-induced signaling, particularly via CaMKII, under conditions of calcium-phosphate dysregulation, is a significant mechanism leading to VSMC pyroptosis.

The findings of the present study and previous research (30) provide strong evidence that NLRP3-dependent pyroptosis in VSMCs is a pivotal event in arterial calcification. While previous research emphasized VSMC apoptosis as a driver of calcification (47,48), recent consensus highlights pyroptosis and phenotypic switching, including the transition to osteochondrogenic cells, as central mechanisms in arterial calcification and atherosclerotic plaque instability (10,49). Given that TUNEL staining, which detects DNA fragmentation, cannot distinguish between apoptosis and pyroptosis (50), additional evidence from GSDMD, caspase-1 and IL-1β cleavage in the present study demonstrated that pyroptosis was the predominant cause and a key upstream event in the calcification process. Notably, genetic deletion of inflammasome components (NLRP3$^{-/-}$, caspase1$^{-/-}$ and GSDMD$^{-/-}$) in mice prevented CM-induced calcification and cell death of the isolated aortic rings, while NLRP3 inhibition significantly reversed CM-induced calcification. This supports the independent roles of NLRP3 and caspase1 in mediating cell death, as their deletion inhibited both cell death and arterial calcification. Furthermore, the results of the present study support that GSDMD cleavage is critical for pyroptotic cell death, with GSDMD deletion also blocking calcification. Given the established link between inflammatory cytokines and vascular calcification, it is plausible that pyroptosis, through the release of VSMC-derived cytokines, serves as the key upstream event mediating CM-induced calcification. Notably, the mechanisms driving intimal calcification in atherogenesis may differ from those underlying medial calcification in chronic renal failure.

The findings of the present study strongly support that Piezo1-CaMKII signaling activation is a critical upstream event in CM-induced pyroptosis and calcification, as inhibition of Piezo1 or CaMKII significantly reversed these processes. CaMKII, as a downstream effector of Piezo1, plays a central role in initiating inflammasome activation and is largely responsible for CM-induced pyroptosis and calcification (37,51). The partial rescue effect observed with CaMKII inhibition could be attributed to its incomplete suppression of CaMKII activity, suggesting the possibility of NLRP3 inflammasome activation via a TLR-independent pathway (52). Furthermore, to the best of our knowledge, the present study provides the first evidence of the binding between CaMKII and RUNX2, reinforcing the conclusion that CaMKII is a key upstream regulator of RUNX2-induced osteoblast differentiation (53,54). However, further research is needed to determine the exact effect of RUNX2-induced osteogenic reprogramming on pyroptosis.

Two major conclusions of the present study are proposed. First, the present study provides the first evidence that Piezo1 activation contributes to high calcium/phosphate-induced calcification in VSMCs. Second, NLRP3 inflammasome-mediated pyroptosis is involved in Piezo1 activation-derived calcification in VSMCs under calcium/phosphate disturbance (Fig. 9). While these findings advance our understanding of vascular calcification mechanisms, several methodological constraints should be noted. The HAD-induced CKD vascular calcification model (55), which mimics VSMC osteogenic transition through mechanisms shared with atherosclerosis (such as oxidative stress and inflammation) (4), enables focused investigation of Piezo1-mediated VSCM osteogenic differentiation. However, although the high calcium/phosphate-induced VSMC osteogenic differentiation model is widely adopted (55), it cannot fully replicate the *in vivo* microenvironment. Therefore, the applicability of these findings to other calcification pathologies, such as atherosclerotic plaque formation or age-related medial calcification, requires further validation due to pathophysiological differences. While the present study has characterized the role of Piezo1 in vascular calcification through *in vitro* models, future studies should utilize RNA interference approaches or Piezo1-selective inhibitors (GsMTx4 or Dooku1) in well-established calcification animal models, such as CKD or vitamin D3 overload models. These investigations would help translate the mechanistic findings of the present study to pathophysiological contexts, while simultaneously assessing therapeutic potential.

Acknowledgements

Not applicable.

Funding

This work was supported by grants from the National Natural Science Foundation of China (grant nos. 82170357 and 82470365) and Natural Science Foundation of Guangdong province (grant nos. 2024A1515010663 and 2021A1515011766).

Availability of data and materials

The data generated in the present study may be requested from the corresponding authors.

Authors' contributions

JT contributed to conceptualization, data curation, formal analysis, methodology, project administration, validation, visualization and writing. DY, ZF and HL contributed to the conception and design of the study, project administration and data validation. YZ, YC and KL contributed to critical intellectual review, identifying key gaps and suggesting additional experiments, validation and project administration. BL and SY contributed to the conception and design of the study as well as project administration. HT contributed to conceptualization, funding acquisition, supervision, project administration and writing. All authors read and approved the final version of the manuscript. JT and HT confirm the authenticity of all the raw data.

Ethics approval and consent to participate

The animal experiments adhered to ethical standards for animal research and were approved by the Ethics Committee of Zhongshan School of Medicine, Sun Yat-sen University (Guangzhou, China; approval no. SYSU-IACUC-2021-000877).

Patient consent for publication

Not applicable.

Competing interests

The authors declare that they have no competing interests.

References

1. Lanzer P, Boehm M, Sorribas V, Thiriet M, Janzen J, Zeller T, St Hilaire C and Shanahan C: Medial vascular calcification revisited: Review and perspectives. Eur Heart J 35: 1515-1525, 2014.
2. Ouyang L, Su X, Li W, Tang L, Zhang M, Zhu Y, Xie C, Zhang P, Chen J and Huang H: ALKBH1-demethylated DNA N6-methyladenine modification triggers vascular calcification via osteogenic reprogramming in chronic kidney disease. J Clin Invest 131: e146985, 2021.
3. Pazár B, Ea HK, Narayan S, Kolly L, Bagnoud N, Chobaz V, Roger T, Lioté F, So A and Busso N: Basic calcium phosphate crystals induce monocyte/macrophage IL-1β secretion through the NLRP3 inflammasome in vitro. J Immunol 186: 2495-2502, 2011.
4. Agharazii M, St-Louis R, Gautier-Bastien A, Ung RV, Mokas S, Larivière R and Richard DE: Inflammatory cytokines and reactive oxygen species as mediators of chronic kidney disease-related vascular calcification. Am J Hypertens 28: 746-755, 2015.
5. Cookson BT and Brennan MA: Pro-inflammatory programmed cell death. Trends Microbiol 9: 113-114, 2001.
6. Toldo S and Abbate A: The NLRP3 inflammasome in acute myocardial infarction. Nat Rev Cardiol 15: 203-214, 2018.
7. Strowig T, Henao-Mejia J, Elinav E and Flavell R: Inflammasomes in health and disease. Nature 481: 278-286, 2012.
8. Shi J, Zhao Y, Wang K, Shi X, Wang Y, Huang H, Zhuang Y, Cai T, Wang F and Shao F: Cleavage of GSDMD by inflammatory caspases determines pyroptotic cell death. Nature 526: 660-665, 2015.
9. Zeng C, Wang R and Tan H: Role of pyroptosis in cardiovascular diseases and its therapeutic implications. Int J Biol Sci 15: 1345-1357, 2019.
10. Burger F, Baptista D, Roth A, da Silva RF, Montecucco F, Mach F, Brandt KJ and Miteva K: NLRP3 inflammasome activation controls vascular smooth muscle cells phenotypic switch in atherosclerosis. Int J Mol Sci 23: 340, 2021.
11. Takahashi M: NLRP3 inflammasome as a common denominator of atherosclerosis and abdominal aortic aneurysm. Circ J 85: 2129-2136, 2021.
12. Ranade SS, Qiu Z, Woo SH, Hur SS, Murthy SE, Cahalan SM, Xu J, Mathur J, Bandell M, Coste B, *et al*: Piezo1, a mechanically activated ion channel, is required for vascular development in mice. Proc Natl Acad Sci USA 111: 10347-10352, 2014.
13. Li J, Hou B, Tumova S, Muraki K, Bruns A, Ludlow MJ, Sedo A, Hyman AJ, McKeown L, Young RS, *et al*: Piezo1 integration of vascular architecture with physiological force. Nature 515: 279-282, 2014.
14. Retailleau K, Duprat F, Arhatte M, Ranade SS, Peyronnet R, Martins JR, Jodar M, Moro C, Offermanns S, Feng Y, *et al*: Piezo1 in smooth muscle cells is involved in hypertension-dependent arterial remodeling. Cell Rep 13: 1161-1171, 2015.
15. Rode B, Shi J, Endesh N, Drinkhill MJ, Webster PJ, Lotteau SJ, Bailey MA, Yuldasheva NY, Ludlow MJ, Cubbon RM, *et al*: Piezo1 channels sense whole body physical activity to reset cardiovascular homeostasis and enhance performance. Nat Commun 8: 350: 350, 2017.
16. Wang S, Chennupati R, Kaur H, Iring A, Wettschureck N and Offermanns S: Endothelial cation channel PIEZO1 controls blood pressure by mediating flow-induced ATP release. J Clin Invest 126: 4527-4536, 2016.
17. Geng J, Shi Y, Zhang J, Yang B, Wang P, Yuan W, Zhao H, Li J, Qin F, Hong L, *et al*: TLR4 signalling via Piezo1 engages and enhances the macrophage mediated host response during bacterial infection. Nat Commun 12: 3519, 2021.
18. Barkai U, Prigent-Tessier A, Tessier C, Gibori GB and Gibori G: Involvement of SOCS-1, the suppressor of cytokine signaling, in the prevention of prolactin-responsive gene expression in decidual cells. Mol Endocrinol 14: 554-563, 2000.
19. Hughes K, Edin S, Antonsson A and Grundstrom T: Calmodulin-dependent kinase II mediates T cell receptor/CD3- and phorbol ester-induced activation of IkappaB kinase. J Biol Chem 276: 36008-36013, 2001.
20. Qian W, Hadi T, Silvestro M, Ma X, Rivera CF, Bajpai A, Li R, Zhang Z, Qu H, Tellaoui RS, *et al*: Microskeletal stiffness promotes aortic aneurysm by sustaining pathological vascular smooth muscle cell mechanosensation via Piezo1. Nat Commun 13: 512, 2022.
21. Liu S, Tao J, Duan F, Li H and Tan H: HHcy induces pyroptosis and atherosclerosis via the lipid raft-mediated NOX-ROS-NLRP3 inflammasome pathway in apoE$^{-/-}$ mice. Cells 11: 2438, 2022.
22. Zeng C, Duan F, Hu J, Luo B, Huang B, Lou X, Sun X, Li H, Zhang X, Yin S and Tan H: NLRP3 inflammasome-mediated pyroptosis contributes to the pathogenesis of non-ischemic dilated cardiomyopathy. Redox Biol 34: 101523, 2020.
23. American Veterinary Medical Association (AVMA). AVMA guidelines for the euthanasia of animals: 2020 Edition. American Veterinary Medical Association; Schaumburg, IL, 2020.
24. Guo Y, Tang Z, Yan B, Yin H, Tai S, Peng J, Cui Y, Gui Y, Belke D, Zhou S and Zheng XL: PCSK9 (proprotein convertase subtilisin/kexin type 9) triggers vascular smooth muscle cell senescence and apoptosis: implication of its direct role in degenerative vascular disease. Arterioscler Thromb Vasc Biol 42: 67-86, 2022.
25. Ayari H and Bricca G: Identification of two genes potentially associated in iron-heme homeostasis in human carotid plaque using microarray analysis. J Biosci 38: 311-315, 2013.
26. Chen YW, Pat B, Gladden JD, Zheng J, Powell P, Wei CC, Cui X, Husain A and Dell'italia LJ: Dynamic molecular and histopathological changes in the extracellular matrix and inflammation in the transition to heart failure in isolated volume overload. Am J Physiol Heart Circ Physiol 300: H2251-H2260, 2011.
27. Durham AL, Speer MY, Scatena M, Giachelli CM and Shanahan CM: Role of smooth muscle cells in vascular calcification: Implications in atherosclerosis and arterial stiffness. Cardiovasc Res 114: 590-600, 2018.
28. Zeng P, Yang J, Liu L, Yang X, Yao Z, Ma C, Zhu H, Su J, Zhao Q, Feng K, *et al*: ERK1/2 inhibition reduces vascular calcification by activating miR-126-3p-DKK1/LRP6 pathway. Theranostics 11: 1129-1146, 2021.
29. Zhang X, Li Y, Yang P, Liu X, Lu L, Chen Y, Zhong X, Li Z, Liu H, Ou C, *et al*: Trimethylamine-N-Oxide promotes vascular calcification through activation of NLRP3 (nucleotide-binding domain, leucine-rich-containing family, pyrin domain-containing-3) inflammasome and NF-κB (nuclear factor κB) signals. Arterioscler Thromb Vasc Biol 40: 751-765, 2020.
30. Pang Q, Wang P, Pan Y, Dong X, Zhou T, Song X and Zhang A: Irisin protects against vascular calcification by activating autophagy and inhibiting NLRP3-mediated vascular smooth muscle cell pyroptosis in chronic kidney disease. Cell Death Dis 13: 283, 2022.
31. Eapen A, Kulkarni R, Ravindran S, Ramachandran A, Sundivakkam P, Tiruppathi C and George A: Dentin phosphophoryn activates Smad protein signaling through Ca2+-calmodulin-dependent protein kinase II in undifferentiated mesenchymal cells. J Biol Chem 288: 8585-8595, 2013.
32. Guan Y, Chen Q, Yang X, Haines P, Pei M, Terek R, Wei X, Zhao T and Wei L: Subcellular relocation of histone deacetylase 4 regulates growth plate chondrocyte differentiation through Ca2+/calmodulin-dependent kinase IV. Am J Physiol Cell Physiol 303: C33-C40, 2012.
33. Jiang M, Zhang YX, Bu WJ, Li P, Chen JH, Cao M, Dong YC, Sun ZJ and Dong DL: Piezo1 channel activation stimulates ATP production through enhancing mitochondrial respiration and glycolysis in vascular endothelial cells. Br J Pharmacol 180: 1862-1877, 2023.
34. Solis AG, Bielecki P, Steach HR, Sharma L, Harman CCD, Yun S, de Zoete MR, Warnock JN, To SDF, York AG, *et al*: Mechanosensation of cyclical force by PIEZO1 is essential for innate immunity. Nature 573: 69-74, 2019.
35. Maldonado N, Kelly-Arnold A, Laudier D, Weinbaum S and Cardoso L: Imaging and analysis of microcalcifications and lipid/necrotic core calcification in fibrous cap atheroma. Int J Cardiovasc Imaging 31: 1079-1087, 2015.
36. Yang Y, Wang D, Zhang C, Yang W, Li C, Gao Z, Pei K and Li Y: Piezo1 mediates endothelial atherogenic inflammatory responses via regulation of YAP/TAZ activation. Hum Cell 35: 51-62, 2022.

37. Szabó L, Balogh N, Tóth A, Angyal Á, Gönczi M, Csiki DM, Tóth C, Balatoni I, Jeney V, Csernoch L and Dienes B: The mechanosensitive Piezo1 channels contribute to the arterial medial calcification. Front Physiol 13: 1037230, 2022.
38. Wang YM, Chu TJ, Wan RT, Niu WP, Bian YF and Li J: Quercetin ameliorates atherosclerosis by inhibiting inflammation of vascular endothelial cells via Piezo1 channels. Phytomedicine 132: 155865, 2024.
39. Kelly-Arnold A, Maldonado N, Laudier D, Aikawa E, Cardoso L and Weinbaum S: Revised microcalcification hypothesis for fibrous cap rupture in human coronary arteries. Proc Natl Acad Sci USA 110: 10741-10746, 2013.
40. Zhang K, Zhang Y, Feng W, Chen R, Chen J, Touyz RM, Wang J and Huang H: Interleukin-18 enhances vascular calcification and osteogenic differentiation of vascular smooth muscle cells through TRPM7 activation. Arterioscler Thromb Vasc Biol 37: 1933-1943, 2017.
41. Ning FL, Tao J, Li DD, Tian LL, Wang ML, Reilly S, Liu C, Cai H, Xin H and Zhang XM: Activating BK channels ameliorates vascular smooth muscle calcification through Akt signaling. Acta Pharmacol Sin 43: 624-633, 2022.
42. Jensky NE, Criqui MH, Wright MC, Wassel CL, Brody SA and Allison MA: Blood pressure and vascular calcification. Hypertension 55: 990-997, 2010.
43. Gudipaty SA, Lindblom J, Loftus PD, Redd MJ, Edes K, Davey CF, Krishnegowda V and Rosenblatt J: Mechanical stretch triggers rapid epithelial cell division through Piezo1. Nature 543: 118-121, 2017.
44. Wang S, Li W, Zhang P, Wang Z, Ma X, Liu C, Vasilev K, Zhang L, Zhou X, Liu L, *et al*: Mechanical overloading induces GPX4-regulated chondrocyte ferroptosis in osteoarthritis via Piezo1 channel facilitated calcium influx. J Adv Res 41: 63-75, 2022.
45. Martinon F, Burns K and Tschopp J: The inflammasome: A molecular platform triggering activation of inflammatory caspases and processing of proIL-beta. Mol Cell 10: 417-426, 2002.
46. Pan X, Xu H, Ding Z, Luo S, Li Z, Wan R, Jiang J, Chen X, Liu S, Chen Z, *et al*: Guizhitongluo Tablet inhibits atherosclerosis and foam cell formation through regulating Piezo1/NLRP3 mediated macrophage pyroptosis. Phytomedicine 132: 155827, 2024.
47. Proudfoot D, Skepper JN, Hegyi L, Bennett MR, Shanahan CM and Weissberg PL: Apoptosis regulates human vascular calcification in vitro: Evidence for initiation of vascular calcification by apoptotic bodies. Circ Res 87: 1055-1062, 2000.
48. Clarke MCH, Littlewood TD, Figg N, Maguire JJ, Davenport AP, Goddard M and Bennett MR: Chronic apoptosis of vascular smooth muscle cells accelerates atherosclerosis and promotes calcification and medial degeneration. Circ Res 102: 1529-1538, 2008.
49. Di C, Ji M, Li W, Liu X, Gurung R, Qin B, Ye S and Qi R: Pyroptosis of vascular smooth muscle cells as a potential new target for preventing vascular diseases. Cardiovasc Drugs Ther: Jun 1, 2024 (Epub ahead of print).
50. Okada K, Naito AT, Higo T, Nakagawa A, Shibamoto M, Sakai T, Hashimoto A, Kuramoto Y, Sumida T, Nomura S, *et al*: Wnt/β-catenin signaling contributes to skeletal myopathy in heart failure via direct interaction with forkhead Box O. Circ Heart Fail 8: 799-808, 2015.
51. Zhang X, Leng S, Liu X, Hu X, Liu Y, Li X, Feng Q, Guo W, Li N, Sheng Z, *et al*: Ion channel Piezo1 activation aggravates the endothelial dysfunction under a high glucose environment. Cardiovasc Diabetol 23: 150, 2024.
52. Cui S, Li Y, Zhang X, Wu B, Li M, Gao J, Xia H and Xu L: FGF5 protects heart from sepsis injury by attenuating cardiomyocyte pyroptosis through inhibiting CaMKII/NFκB signaling. Biochem Biophys Res Commun 636: 104-112, 2022.
53. Li Y, Ahrens MJ, Wu A, Liu J and Dudley AT: Calcium/calmodulin-dependent protein kinase II activity regulates the proliferative potential of growth plate chondrocytes. Development 138: 359-370, 2011.
54. Yu L, Ma X, Sun J, Tong J, Shi L, Sun L and Zhang J: Fluid shear stress induces osteoblast differentiation and arrests the cell cycle at the G0 phase via the ERK1/2 pathway. Mol Med Rep 16: 8699-8708, 2017.
55. Yang L, Dai R, Wu H, Cai Z, Xie N, Zhang X, Shen Y, Gong Z, Jia Y, Yu F, *et al*: Unspliced XBP1 counteracts β-catenin to inhibit vascular calcification. Circ Res 130: 213-229, 2022.

Copyright © 2025 Tao et al. This work is licensed under a Creative Commons Attribution-NonCommercial-NoDerivatives 4.0 International (CC BY-NC-ND 4.0) License.